

Groundwater for Sustainable Development

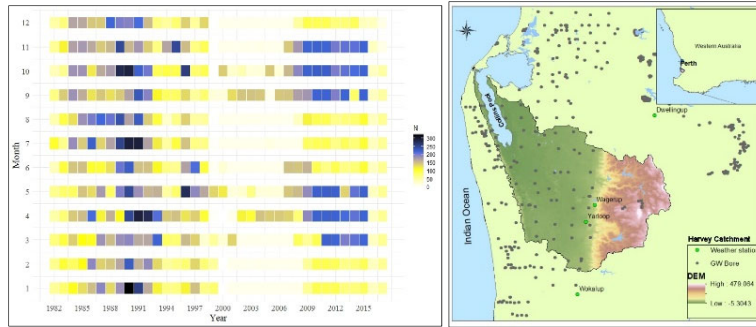
Evaluation of non-uniform groundwater level data using spatiotemporal modeling

--Manuscript Draft--

Manuscript Number:	GSD-D-21-00108R1
Article Type:	Research Paper
Keywords:	Spatiotemporal Regression Kriging; Non-uniformly distributed data; Groundwater level; Leave-One-Out Cross-Validation; Time-series analysis; Data-scarce catchments
Corresponding Author:	Hamideh Kazemi Curtin University Bentley Campus: Curtin University AUSTRALIA
First Author:	Hamideh Kazemi
Order of Authors:	Hamideh Kazemi Ranjan Sarukkalige Quanxi Shao
Abstract:	<p>Groundwater is one of the main sources of freshwater. To ensure its sustainability, it is important to know its current status and changing pattern over time, through the essential groundwater monitoring program conducted by water management planners, groundwater modelers and urban developers. However, uniformly distributed data is hardly available in most catchments. In this study, the Spatiotemporal Regression Kriging method (Rkriging) was adopted to derive a spatiotemporal pattern for Harvey River Catchment in Western Australia, using the limited groundwater data in the catchment. The accuracy of the estimation was investigated using the Leave-One-Out Cross-Validation approach. Time-series analysis (i.e., auto-correlation and cross-correlation) was then employed to provide a better understanding of the estimated groundwater level change (ΔGWL) over time. To gain insight into the change of groundwater levels, the correlation between groundwater level (GWL) and precipitation pattern with possible time-lag was explored. The results showed that the Rkriging method is satisfactory and the findings were consistent with the previously published results in literature in the area. The estimated decreasing GWL trend matched the precipitation pattern in the catchment. Such shallow groundwater levels in Harvey Catchment resulted in a short time-lag between the precipitation and GWL time-series. The proposed method should be applied to other catchments with limited groundwater data and can be a useful approach for catchments with irregular temporal and spatial data.</p>
Suggested Reviewers:	Fariborz Masoumi, Dr Lecturer, University of Mohaghegh Ardabili f_masoumi@uma.ac.ir Mohammad Javad Emami Tehran University: University of Tehran mje.skardi@ut.ac.ir So Kazama, Professor Tohoku University: Tohoku Daigaku so.kazama.d3@tohoku.ac.jp
Opposed Reviewers:	
Response to Reviewers:	

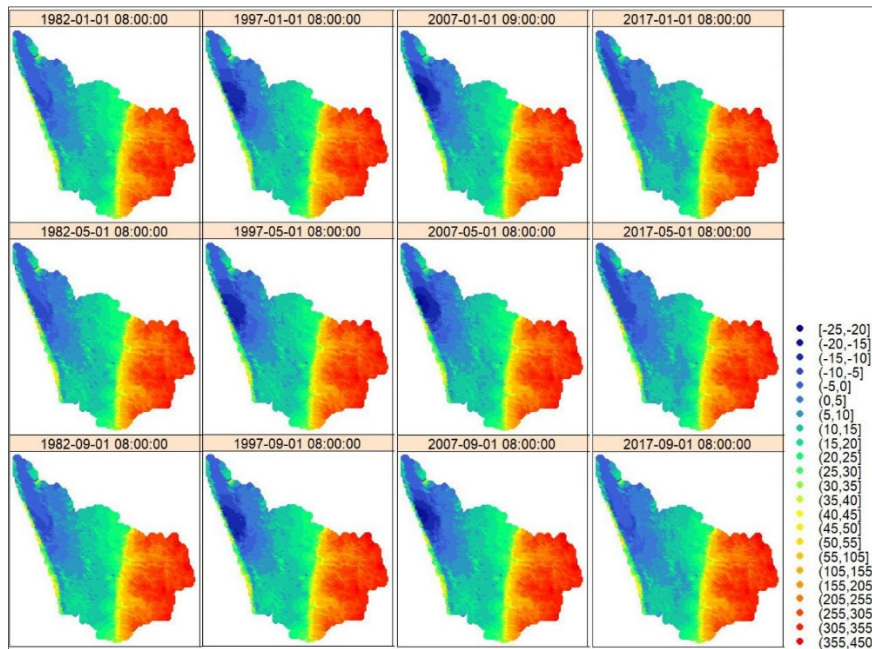
Highlights:

- Spatiotemporal kriging model is constructed to estimate groundwater level from non-uniformly distributed data
- The model performance is assessed using Leave-One-Out Cross validation
- The association between groundwater level change and rainfall is explored
- The framework is applicable to any other catchments, particularly, catchments in data-scarce regions



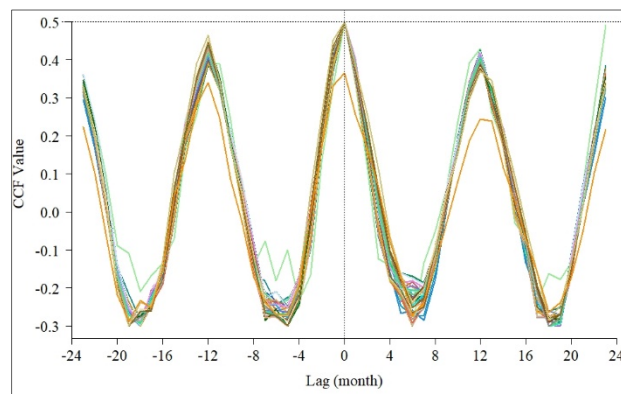
Input: Non-uniform spatial and temporal groundwater level (GWL) data, Harvey Catchment, AU

Regression kriging method



Output: Monthly GWL data and associated maps for the study period (1982-2018)

Time-series analysis



Short time-lag is detected between Δ GWL and Precipitation

1 Evaluation of non-uniform groundwater level data using spatiotemporal modeling

2 Hamideh Kazemi^{1,2†}, Ranjan Sarukkalige¹, and Quanxi Shao²

3 ¹School of Civil and Mechanical Engineering, Curtin University, Perth, Australia

4 ²CSIRO Data 61, Kensington, WA 6151, Australia

5

6 *Corresponding author:* Hamideh Kazemi (hamideh.kazemi@postgrad.curtin.edu.au)

7 †<https://orcid.org/0000-0002-9088-0958>.

8

9 Abstract

10 Groundwater is one of the main sources of freshwater. To ensure its sustainability, it is
11 important to know its current status and changing pattern over time, through the essential
12 groundwater monitoring program conducted by water management planners, groundwater
13 modelers and urban developers. However, uniformly distributed data is hardly available in
14 most catchments. In this study, the Spatiotemporal Regression Kriging method (Rkriging) was
15 adopted to derive a spatiotemporal pattern for Harvey River Catchment in Western Australia,
16 using the limited groundwater data in the catchment. The accuracy of the estimation was
17 investigated using the Leave-One-Out Cross-Validation approach. Time-series analysis (i.e.,
18 auto-correlation and cross-correlation) was then employed to provide a better understanding of
19 the estimated groundwater level change (Δ GWL) over time. To gain insight into the change of
20 groundwater levels, the correlation between groundwater level (GWL) and precipitation
21 pattern with possible time-lag was explored. The results showed that the Rkriging method is
22 satisfactory and the findings were consistent with the previously published results in literature
23 in the area. The estimated decreasing GWL trend matched the precipitation pattern in the
24 catchment. Such shallow groundwater levels in Harvey Catchment resulted in a short time-lag
25 between the precipitation and GWL time-series. The proposed method should be applied to
26 other catchments with limited groundwater data and can be a useful approach for catchments
27 with irregular temporal and spatial data.

28

29 Keywords

30 Spatiotemporal Regression Kriging; Non-uniformly distributed data; Groundwater level;
31 Leave-One-Out Cross-Validation; Time-series analysis; Data-scarce catchments

32

33 **1 Introduction**

34 Groundwater produces almost 30% of known freshwater resources worldwide and
35 almost 96% of non-solid freshwater (Green et al., 2011). As groundwater is less sensitive to
36 the immediate climate variation, it is a great water source to overcome droughts and mitigate
37 climate change impacts on limited freshwater resources. However, excessive groundwater
38 discharge and lack of enough recharge threaten the existence of these precious freshwater
39 systems (Green et al., 2011). Regular monitoring program is usually conducted to understand
40 the changing pattern of groundwater and help proposing effective groundwater management
41 and decision-making plans. However, due to the costs and accessibility, only limited sites are
42 monitored, resulting in sparse data series over the catchments, discontinuous sites and missing
43 observations within sites. The lack of regular measurements, which results in spatiotemporal
44 data gaps, can disturb our understanding of the catchment (Ruybal et al., 2019; Varouchakis &
45 Hristopulos, 2013). To better understand the status and changing patterns of groundwater levels
46 (GWL) for both management and research purposes, uniformly distributed GWL are necessary.
47 This, only, can be achieved by filling the gaps (that is, estimating the missing values in space
48 and time) through interpolation methods (Varouchakis & Hristopulos, 2013), which have been
49 widely used in many research areas; for instance, rainfall pattern prediction (Goovaerts, 2000),
50 climate parameters estimation (Haylock et al., 2008), spatial analysis of groundwater quantity
51 and quality (Dash et al., 2010) and spatial variability of GWL (Varouchakis & Hristopulos,
52 2013; Yao et al., 2014). Most of these studies, however, explored either spatial or temporal
53 aspect of the subjects and not the interplay between time and space; while due to the changing
54 environment, geohydrological parameters, such as groundwater, are subject to change in time
55 and space (Varouchakis & Hristopulos, 2019). To accurately take account of these changes,
56 the employed method should consider the interdependency between temporal and spatial
57 aspects of the parameters. From modelling perspectives, simultaneously considering both the
58 irregularly sampled spatial and temporal data can best use the available information. One of
59 the popular interpolation methods is spatiotemporal regression kriging (Rkriging) which has
60 been applied to variables in different catchments and will be used for this purpose. The
61 Rkriging uses spatial and temporal correlations between observed (sampled) points to estimate
62 the un-sampled spatiotemporal locations (Hu et al., 2017; Adigi 2019). The model, unlike most
63 interpolation methods, performs well for un-sampled locations or where uniform data is not
64 available (Hu et al., 2017; Adigi 2019). The Rkriging, unlike techniques such as spline
65 interpolation, can interpret the geostatistical aspect of the parameter (Hengle et al., 2012) where

66 the variability of the parameter in space and time is modeled by adding the temporal element
67 to the spatial domain. Hu et al (2017) used spatiotemporal regression kriging (Rkriging) to
68 predict precipitation trend in Uygur region, where the station data is sparse and unevenly
69 distributed. They chose Normalized Difference Vegetation Index (NDVI), Digital Elevation
70 Model (DEM) and a temporal index as the model's regressors. The model was able to
71 successfully detect a pattern in precipitation, and successfully reveal the correlation between
72 precipitation and altitude (Hu et al., 2017). In another interesting research, Ruybal et al (2019)
73 used Rkriging to predict groundwater level at ungauged locations in Arapahoe aquifer and
74 showed that the Rkriging method is a competent approach to estimate the GWL. The model
75 was able to produce realistic values and Rkriging showed to be superior to the traditional
76 kriging method (Ruybal et al., 2019).

77 The spatial and temporal dependency of the studied parameter (here, GWL) is called
78 empirical variogram. The interpolation models, including kriging, fit a surface to the empirical
79 variograms and produce modeled variograms (here after called variograms). Fitting the optimal
80 variograms is the first and most important step for conducting an accurate spatiotemporal
81 analysis. Adding temporal domain to the spatial interpolation, usually, results in a more
82 accurate and realistic modeling, however it can increase the complexity of the model. For
83 instance, the temporal and spatial structure of the variogram are not necessary the same. The
84 spatial and temporal variograms can follow different covariance functions and patterns (Graler
85 et al., 2016; Voss et al., 2016). Earlier spatiotemporal variograms (STvariogram) were built of
86 separate spatial and temporal domains. These domains werelater added or multiplied together,
87 to form the final spatiotemporal variogram. These variograms, called separable, are simpler but
88 based on unrealistic assumptions (Varouchakis & Hristopulos, 2019); therefore, non-separable
89 variograms have been developed and were applied in many fields, including hydrogeology. For
90 instance, Guo et al (2014) applied three non-separable spatiotemporal variogram models (i.e.,
91 Cressie–Huang model, Gneiting model and product-sum model) to predict the green gas
92 emission over China, during 2009-2012. They compared these variogram models with the
93 empirical variogram surface, and showed that the product-sum model predicts slightly better
94 than the rest. However, the three models were almost equally capable of generating column-
95 averaged carbon dioxide dry air mole fractions (X_{CO_2}) concentration maps (Guo et al., 2014).

96 In the current research, spatiotemporal regression kriging (Rkriging) method is adopted
97 to investigate GWL, in the highly important Harvey Catchment in Western Australia, where
98 the historical observed data were spatially and temporally irregular. The catchment is one of
99 the main water sources for the Perth metropolitan (Al-Safi et al., 2020). It is home to a vast

100 range of groundwater-dependent biodiversity, and its wetlands and lakes are in the list of
101 wetlands of international importance (Environmental Protection Authority, 2008). The
102 proposed method produces spatiotemporal maps for the catchment to track the groundwater
103 change during the study period of 1982-2017. To choose the best spatiotemporal variogram,
104 for a given sample set, several variograms are compared; to find the optimum number of spatial
105 and temporal observations, different spatiotemporal sampling sizes are investigated. The whole
106 catchment is divided into fine grids and for each grid a monthly timetable is provided to
107 overcome non-uniformity due to the temporal and spatial gap in the observed data.

108 As the catchment information (such as location and elevation) can be highly corrected,
109 direct use of this data may make the model too sensitive. Correlated covariates can affect the
110 significance of the variables, and their interdependence can make the estimation sensitive to
111 minor changes which might introduce imprecise regression coefficients and accordingly higher
112 errors to the model. Therefore, Principal Component Analysis (PCA) is performed to prevent
113 multi-collinearity in the covariates and to avoid information overlapping. The PCA is a
114 common method that transforms the covariates into orthogonal and uncorrelated components.
115 It reduces the original variables to a limited number of integrated variables, which explain most
116 of the variance (Ruybal et al., 2019). The stepwise regression algorithm is, also, used to select
117 the most significant regressors. The accuracy of the Rkriging method is examined by the Leave-
118 One-Out-Cross validation technique.

119 After studying groundwater change in the catchment, it is interesting to explore the
120 possible reason behind the change. Although precipitation is one of the main factors affecting
121 GWL, its impact on GWL is not fully understood (Kotchoni et al., 2019), mainly due to lack
122 of enough GWL information and complicated structure of groundwater. Time-series analysis
123 (i.e., cross-correlation and auto-correlation) is a common approach to investigate correlation
124 between hydrological time-series (Cai & Offerdinger, 2016; Duvert et al., 2015; John & John,
125 2019; Kim & Lee, 2017; Lee et al., 2006; Lehmann & Rode, 2001; Shi et al., 2019). The cross-
126 correlation analysis provides useful information regarding the significance and the first
127 response of the groundwater resources to precipitation. Auto-correlation analysis, on the other
128 hand, reveals structure of the time-series and impact of memory effect. In this paper, the
129 correlation between the estimated groundwater and observed precipitation time-series with
130 possible lags is examined at a randomly selected number of points, to investigate the
131 interdependency between GWL and precipitation time-series, and detect any possible time-lag.

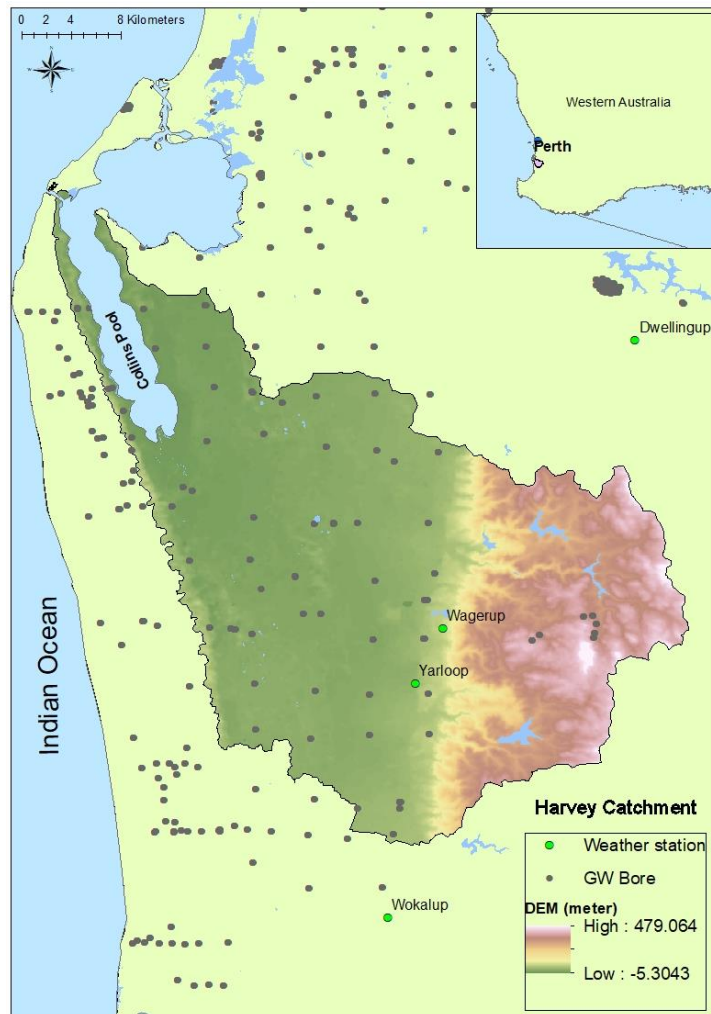
132 The paper is organized as follows. The study area and data set are described in Section
133 2, followed by the methodology. The results and model assessment in relation to the data set
134 are given in section 4. In section 5, conclusions and a discussion are drawn from this study.

135 **2 Study area and data**

136 Harvey River Catchment with size of 1041 km² is located at 130 km south of Perth city
137 in Western Australia. The Harvey River is one of the most important water sources for Perth
138 metropolitan area. The catchment, as a part of the bigger Peel-Harvey basin, is internationally
139 recognized as the main water-birds place in south west of Australia (Kelsey et al., 2010; Ruibal-
140 Conti, 2014). It has a Mediterranean climate with hot-dry summers and cold-wet winters.
141 Harvey catchment has experienced one of the fastest development and urbanization in Western
142 Australia, especially in the coastal areas (Kazemi et al., 2019; Kelsey et al., 2010).

143 Almost all climate scenarios (GCMs) predicted hotter and drier climate for south
144 Western Australia, for the next decades (Ali et al., 2012; CSIRO, 2009). Direct impacts of
145 hotter and drier climate on GWL is variation of streamflow and precipitation, and accordingly,
146 decreasing groundwater recharge. Climate change can also affect GWL indirectly, by reshaping
147 groundwater users' daily routine (Taylor et al., 2013). Three main recharge mechanisms
148 affecting groundwater system are direct recharge (e.g., infiltration resulted from precipitation),
149 indirect recharge (e.g., infiltration from surface water), and localized recharge (e.g.,
150 concentrated surface water such as lakes and agricultural area) (De Vries & Simmers, 2002).
151 In the case of Harvey catchment, where studies show the precipitation has decreased during
152 the last decades, sandy soil structure of the area makes precipitation infiltration the only reliable
153 means to replenish the water table. Groundwater consumption routine, on the other hand, has
154 changed dramatically, from a very limited percentage during the 1960s to almost equal as
155 surface water in 1985. Nowadays, more than 75% of water originates from groundwater in the
156 area. Excessive water withdrawal for domestic, agricultural and industrial purposes, has
157 affected the GWL, and therefore, has manipulated the dependent ecosystem (Ali et al., 2012;
158 CSIRO, 2009).

159 The required groundwater and climate data are available on the Bureau of Meteorology
160 (BOM) of Australia's website (BoM, 2020). The groundwater data were collected from
161 monitoring wells for the period of 1982 to 2017, where the reference point is the mean sea
162 level. The temporal and spatial availability of the data is highly non-uniform in the catchment.
163 As presented in Figure 1 monitoring wells are unevenly scattered through the catchment. In the
164 south-eastern part of the catchment, for instance, there are very few wells available.



166

167

Fig.1 Locations of groundwater wells and weather stations in Harvey Catchment

168

169

170

171

172

The temporal distribution of the data is also not uniform. Many wells were operating only for limited years, some of the wells provide annual data and some monthly data (Fig.2). As presented in Fig.2, very few information is available in some years (e.g., 2000-2008). In this study, it is assumed that the temporal trend within the study period continues and is not affected by dramatic human-induced changes.

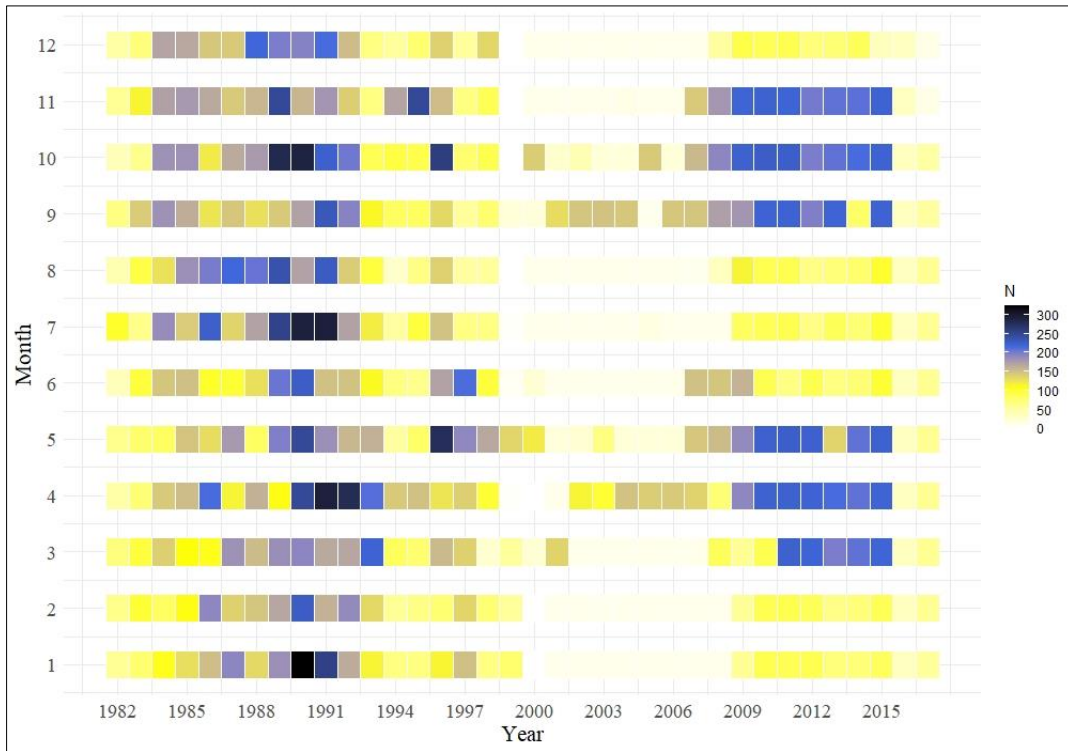


Fig.2 Heatmap of the available data showing non-uniform temporal distribution of the GWL information in the Harvey Catchment. N is number of available data in a month.

173
174
175

176 3 Methodology

177 Spatiotemporal Regression Kriging (Rkriging) predicts the spatial and temporal links
178 between observed values. In this method, the regression (deterministic) and residual
179 (stochastic) parts of the model are analyzed separately (Eq. (1)).

180

$$181 \quad Z(s, t) = m(s, t) + \varepsilon(s, t) + r \quad (1)$$

182 where $Z(s, t)$ is the observed GWL at space (s) and time (t), $m(s, t)$ is the trend
183 (deterministic) component, $\varepsilon(s, t)$ is residual (stochastic) component of the model, which is the
184 spatiotemporally auto-correlated residual for every $(s, t) \in S \times T$ where $S \subset \mathbb{R}^2$ is the spatial
185 domain and $T \subset \mathbb{R}$ is the temporal domain (Varouchakis & Hristopulos, 2019), and r is the
186 uncorrelated noise (Hu et al., 2017; Ruybal et al., 2019). The regression method is applied to
187 predict the values on a fine grid. This part of the analysis, which called trend analysis, gives a
188 rough estimation for each grid. Then, the residuals are extracted by deducting the trend from
189 the observed data. For the residual part, the best spatiotemporal variogram (STvariogram) is
190 fitted and the interpolated residuals for all grid values are calculated. Finally, the two
191 components (trend and residual) are added back, to provide the final estimation of the GWL

192 (Hu et al., 2017). All of the analysis and codes are developed and performed in Rstudio
193 platform.

194 3.1 RKriging of the residuals

195 The sample spatiotemporal semi-variogram (which is half the empirical STvariogram)
196 is produced using the residuals as follow (Hu et al., 2017):

$$197 \gamma(h, u) = \frac{1}{2N(h, u)} \sum_{i=1}^{N(h, u)} [\varepsilon(s, t)_i - \varepsilon((s + ht)_i, (h + u))]^2 \quad (2)$$

199 where h is the separation distance for points in space, u is the separation in time, and
200 $N(h, u)$ is the number of paired observations of z separated by lag (h, u) . A model is fitted after
201 the sample STvariogram is determined. Among the several models to estimate STvariogram,
202 separable, Product-sum, and sumMetric models are the most common (Hu et al., 2017; Ruybal
203 et al., 2019; Varouchakis & Hristopulos, 2019). The separable model, belongs to the separable
204 covariance models, assumes that space and time domains of the variogram are separate and
205 treats them independently, while product-sum and sumMetric models, belong to the non-
206 separable covariance models, consider the interaction between space and time components.
207 The advantages of the separable models are computationally fast with few parametrization,
208 however these models cannot fully grasp the complicated interaction between the spatial and
209 temporal components (Hengl et al., 2012; Geniaux, 2017; Varouchakis & Hristopulos, 2019).
210 Therefore, in the current study, models from both separable and non-separable groups are
211 selected and the results are compared to choose the best fit for the sample (empirical)
212 spatiotemporal variogram.

213 3.2 Leave-One-Out Cross-Validation (LOOC)

214 To investigate the accuracy of the regression kriging, the Leave-One-Out Cross-
215 Validation (LOOC) method is applied. A code is written in R to perform the spatiotemporal
216 cross validation. During this process, for each space-time data is removed once, the remaining
217 data are used to calibrate the model which is used to predict the value of the removed point.
218 This process is repeated for all values in the data pool. Finally, the predicted values and
219 observed values are compared to examine the accuracy of the prediction (Learning E.o.M,
220 2010).

221 3.3 Principal Component Analysis (PCA)

222 In this study, the built-in R functions `prcomp()` is used to perform the PCA. This
223 function determines rotation and shift of the original data to a new coordinate system, in which
224 the covariates are independent. For the current work, the two groups of covariates for PCA
225 analysis are Harvey digital elevation model (DEM) and the extended boundary of the
226 catchment (i.e., Longitude and Latitude of the catchment), as suggested by (Ruybal et al.,
227 2019).

228 3.4 Time-series Analysis

229 Time-series analysis is carried out, for forty randomly selected grid points, to better
230 understand interrelationship between estimated GWL and groundwater level change (Δ GWL),
231 and precipitation time-series. The Cross-Correlation function (CCF) provides time-lag between
232 the input and output, which suggests the response time of the output time-series. Equations 3
233 and 4 represent the mathematical expression of the CCF (Cai & Offerdinger, 2016; Shi et al.,
234 2019).

$$235 \quad C_{xy}(k) = \frac{1}{n} \sum_{t=1}^{n-k} (x_t - \bar{x})(y_{t+k} - \bar{y}) \quad (3)$$

$$236 \quad \Gamma_{xy}(k) = \frac{C_{xy}(k)}{\sigma_x \sigma_y} \quad (4)$$

237 where $C_{xy}(k)$ is the cross-covariance between x_t (input time-series) and y_t (output time-
238 series), k and n are the time-lag and the length of the time-series, respectively, and σ is the
239 standard deviation of x and y .

240 The Auto-Correlation Function (ACF), on the other hand, is cross-correlation of the
241 time-series with itself, at different time-lags. This parameter provides the “memory effect” of
242 the dataset, which shows interdependency of the time-series to its historical values. For an
243 uncorrelated time-series, the ACF shows sharp decrease within a short period, while a gradual
244 decline shows strong interdependency and a long memory effect (Cai & Offerdinger, 2016;
245 Larocque et al., 1998).

246 4 Results

247 The study area is divided into 450×450 meter grids. For each grid a monthly temporal
248 data-frame is provided to produce a uniform spatiotemporal structure and cover the temporal
249 and spatial gaps in the observed data.

250 4.1 PCA calculation

251 As presented in Table 1, the PCA conversion of the original covariates (i.e., longitude,
252 latitude and elevation) explained more than 96% of the variance with two components (i.e.
253 PCA1 and PCA2).

254

255 **Table 1** PCA conversion of the original covariates longitude, latitude and elevation explaining 96% of the variance

Parameters	PCA1	PCA2	PCA3
Standard deviation	1.375	0.9998	0.332
Proportion of Variance	0.63	0.33	0.04
Cumulative Proportion	0.63	0.96	1

256

257 As the difference between the variables' ranges and magnitudes might introduce bias
258 to the analysis, all the values were scaled before being projected to the new coordinate system
259 (i.e., PCA provided coordinates). A stepwise regression analysis was performed to provide the
260 subset of optimum regressors, which best describe the trend component. The stepwise
261 regression showed that among the various combinations of the potential predictors (i.e., PCA1,
262 PCA2, latitude (Lat), longitude (Long), Elevation (Elev), Year the measurement was taken,
263 and Month the measurement was taken), PCA1 and Long give the optimum combination.
264 Hence, the trend component of GWL in the Harvey catchment has only the spatial dimension
265 (Eq. (5)):

266

267
$$m(s) = -4.227 \times Long + 2.398 \times PCA1 + 1740.142 \quad (5)$$

268 Augmented Dickey-Fuller test for stationarity was used to check the stationarity of the
269 input times-series. The test showed that before the trending decomposition the data was non-
270 stationary with p-value = 0.3 and after decomposing and trend deduction, the residual became
271 stationary with the p-value = 0.01.

272

273 4.2 Spatiotemporal variogram (STvariogram) model for residuals

274 Each component of the STvariogram can be described by a model such as spherical,
275 exponential, Gaussian or Wave models. Different configuration of these models were tested
276 for three widely used STvariograms (i.e., Separable, Product-sum and sumMetric), to
277 determine the best model. Based on the least mean square value, the combination of the
278 Exponential and Gaussian models were chosen for spatial and temporal components of the

279 STvariograms, respectively. For the joint component of the sumMetric STvariogram, the
 280 Exponential model was the best option (table 2). The initial values of sill, range and nugget
 281 were chosen based on the sample spatial and temporal variograms and then adjusted to
 282 minimize the mean square error between the sample and modeled STvariogram. In this case
 283 study, the directional sample variogram did not show strong anisotropic behavior, therefore the
 284 value of anisotropy (k) is set to minimum.

285

286 **Table 2** Parameters of the fitted models and comparison of the goodness of fit to choose the best STvariogram

Variogram components	Model	Sill (km)	Range (km/day)	Nugget (km ²)	MSE (mean square error)		
					Separable	Product-sum	sumMetric
Spatial	Exponential	60	10	0	231	212	209
Temporal	Gaussian	50	1000	0			
Joint (only for sumMetric)	Exponential	80	20	40			

287

288 Fit.StVariogram function in the gstat package was used to fit the model against the
 289 empirical variogram from sample. The embedded L- BFGS- B algorithm was used to
 290 minimize the error between the model and the sample. The aforementioned algorithm is an
 291 extension of the Limited-memory BFGS optimization algorithm which belongs to Quasi-
 292 Newton methods. It is one of the most popular and efficient algorithms for fitting kriging
 293 models which allows to impose simple box constraints on the variables for numerical
 294 optimizations (Guitton, 2004).

295 The optimum number of spatiotemporal observations was determined by trial and error
 296 method. Comparing the STvariograms with the empirical variogram surface showed that both
 297 spatial closeness and number of available data in individual wells, play important roles in
 298 accuracy of the variograms. Congested number of wells in one location causes overfitting and
 299 scattered temporal data leads to unrealistic variogram. Finally, 641 wells, with at least 10
 300 available temporal data, were selected, for this study.

301 As suggested in Table 2, the two non-separable models perform better than the
 302 separable model implying importance of the link between the spatial and temporal domains of
 303 the variogram. Among the three employed models, the sumMetric model outperforms the other
 304 STvariograms with lower Mean Square Error Value (MSE). The sumMetric model is a
 305 combination of sum and metric models (Eq.6) (Derakhshan & Leuangthong, 2006;
 306 Dimitrakopoulos & Luo, 1994; Rouhani & Hall, 1989).

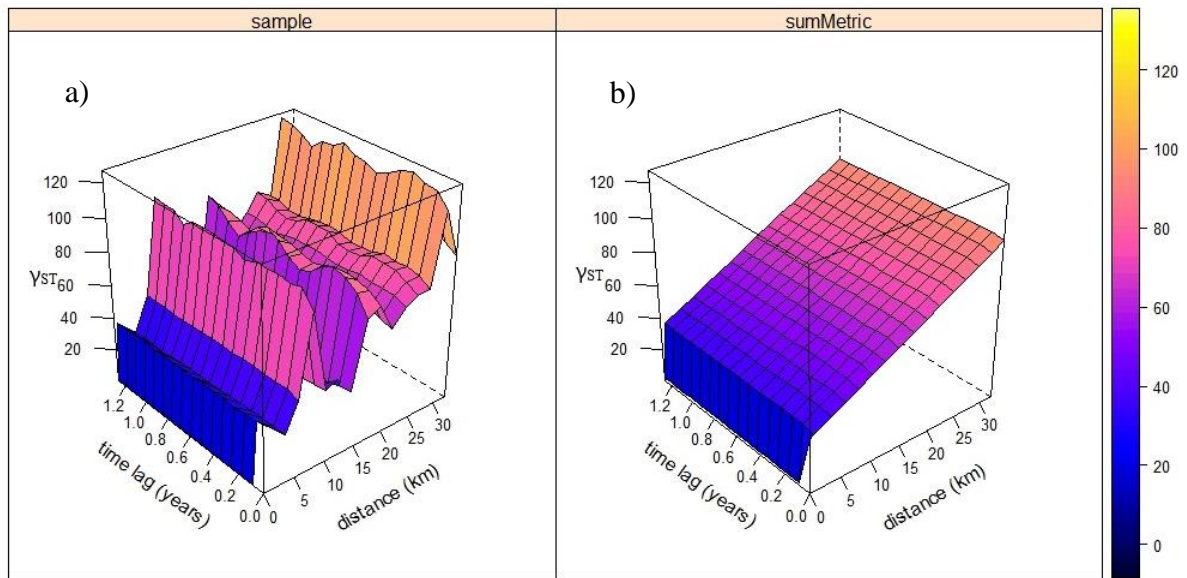
307

308 $\gamma_{ST}(s, t) = \gamma_S(h) + \gamma_T(u) + \gamma_J(\sqrt{h^2 + (\kappa u)^2})$ (6)

309 where κ is the spatio-temporal ratio of anisotropy, which combines spatial distances
310 with temporal distances, and $\gamma_S, \gamma_T, \gamma_J$ are the spatial, temporal, and joint components of the
311 STvariograms, with separate nugget effects.

312 Figure 3 compares the empirical surface variogram and the best fitted STvariograms
313 (i.e., sumMetric estimated STvariogram). The general increasing tendency of gamma-ST (γ_{ST})
314 with distance suggest that the correlation between the residuals decreases as the distance
315 between the wells increases. The value of γ_{ST} , however, shows less sensitivity to time-lag.

316

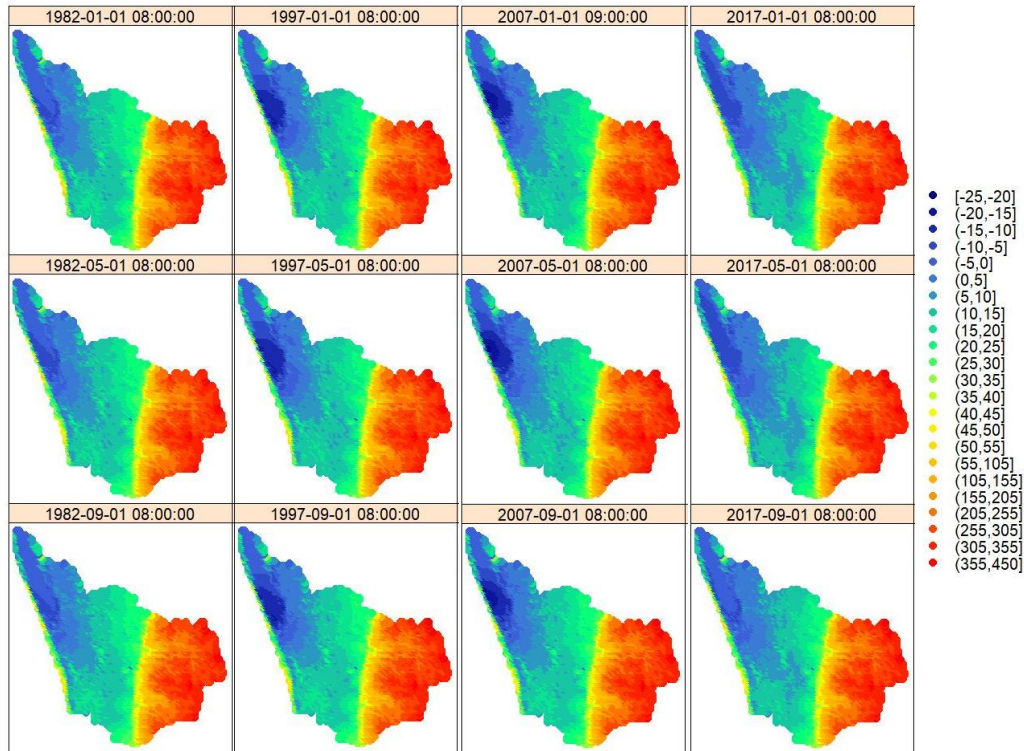


317

318 **Fig.3** a) the empirical surface of the GWL residuals after trend removal and b) the fitted spatio-temporal variogram of the residuals using
319 sumMetric model

320 4.3 Spatiotemporal Kriging Predicted Groundwater Levels

321 The trend (determinist component) and residual (stochastic component) together
322 provide the final estimation of the GWL at any grid points in each month, based on which
323 monthly GWL maps can be produced for the study years (i.e., 1982-2017). For the sake of
324 presentation, Figure 4 presents only the maps for selected months of January, May and
325 September in the selected years of 1982, 1997, 2007 and 2017. As expected, the deeper water
326 table is located in south-eastern part of the catchment and shallower water table (the dark blue
327 color) is in the coastal area (i.e., the north-western part, where the catchment meets the sea). It
328 is also shown that GWL follows the same trend over the years although the actual GWL at each
329 grid vary from year to year.

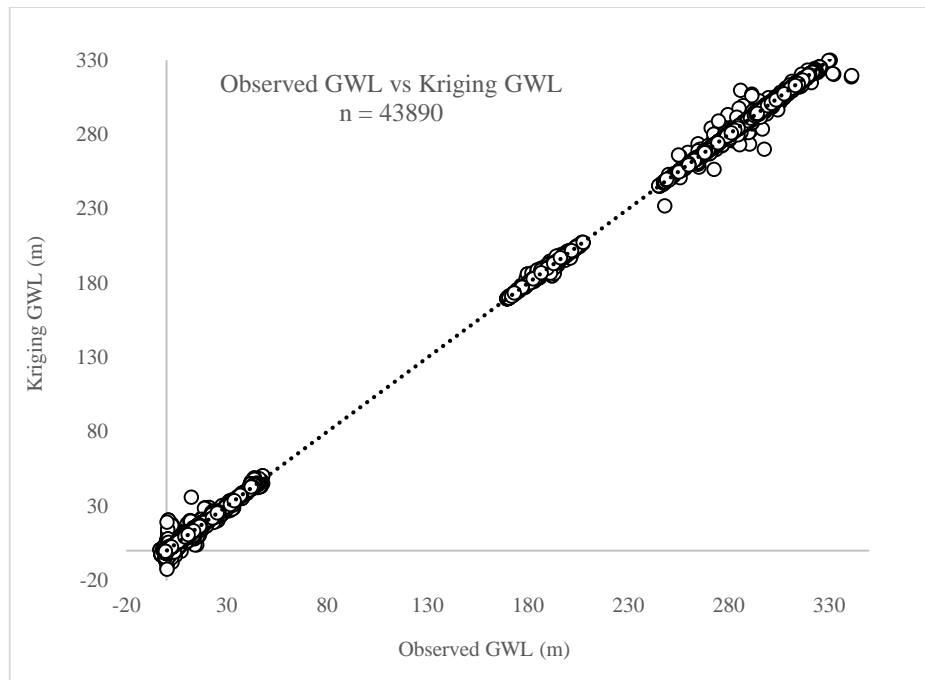


330
 331 **Fig.4** Created maps of estimated Harvey catchment GWL (m) for selected months of the study period (1982-2018) where hot
 332 and cold colors representing deeper and shallower groundwater level, respectively

333 4.4 Cross-validation

334 The “Leave- one- out” cross- validation was carried out for almost 44000
 335 spatiotemporal data points to compare the estimated values with the observed values (Figure
 336 5). These spatiotemporal points are the observed GWL data from the wells, during the 36 years
 337 of study period. Non-uniformity of the observed data can also be observed from the figure
 338 where there is a lack of information within some ranges of elevation. The diagram suggests the
 339 Rkriging method is well capable of estimating GWL in the catchment, with the R-square value
 340 very close to 1 (i.e., 0.99).

341



342

343

344

Fig.5 Leave–One-Out Cross Validation result showing the goodness of fit between Rkriging predicted GWL and observed GWL information from the 641 wells in the Harvey Catchment.

345

4.5 Time-series Analysis

346

347

348

349

350

351

352

353

354

355

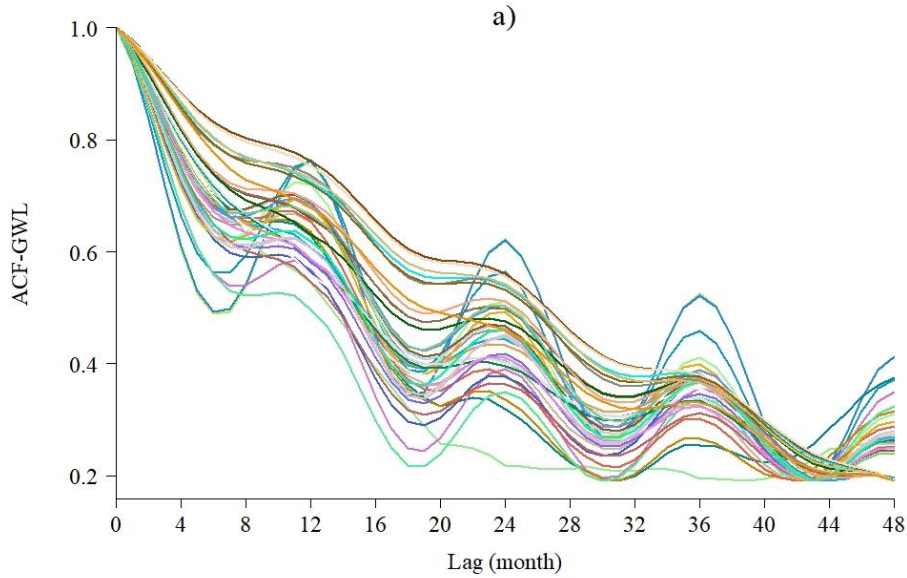
356

357

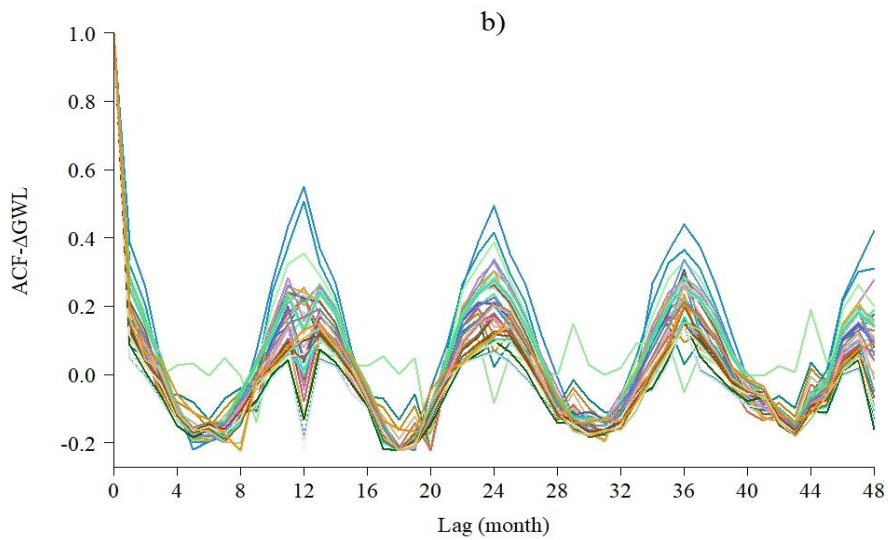
358

359

Forty randomly selected samples (as hypothetical wells) were chosen to perform the auto-correlation and cross-correlation analysis. The samples are almost uniformly distributed in the catchment and cover all of the elevation classes. Figure 6 shows the values of auto-correlation function for GWL and Δ GWL. The gradual decline in the ground water level indicates the autocorrelation can last for at least four years (ACF above 0.2). Those samples which show sinusoidal, yet gradually decreasing patterns, are mainly located on the Collins Pool or very close to the pool. The ACF for Δ GWL shows completely different behavior and decreases rapidly which implies the effect of historical data naturally declines over time. For most of the cases, the ACF graphs for Δ GWL does not decrease with increasing lag and follow a sinusoidal pattern with 12 month circle, however, the seasonality and correlation are negligible. The aforementioned samples, located on or close to the Collins pool, perform higher seasonal auto-correlation values, indicating stronger impact of historical values and memory effect. As the pool is connected to the ocean (Figure 1), the unusual trend (i.e., stronger seasonal interdependency) of these samples can be because of the influence of ocean water.



360



361

362

363

Fig.6 a) Auto Correlation Function (ACF) for GWL and b) Δ GWL in 48 months showing the autocorrelation values between the time-series

364

365

366

367

368

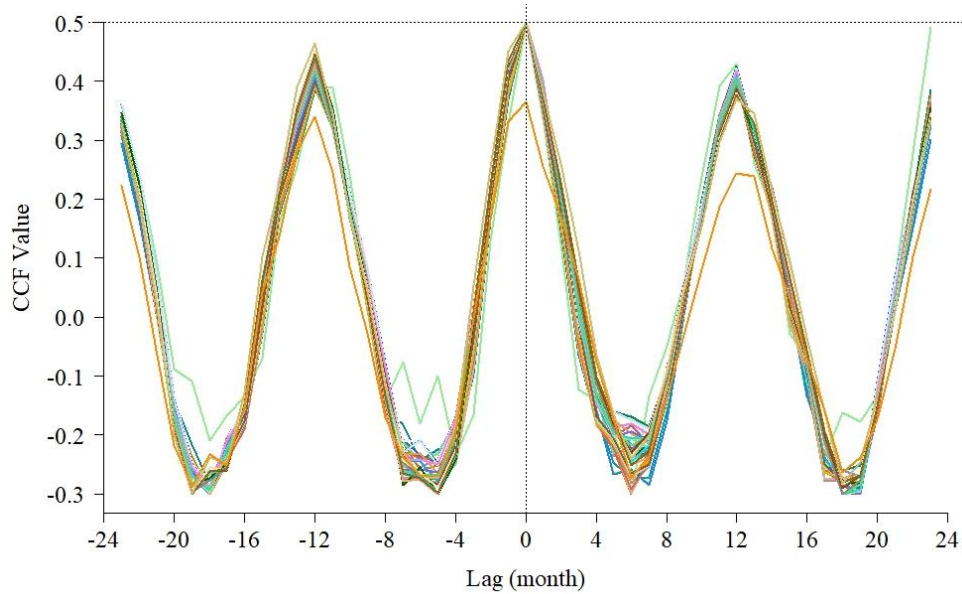
369

370

371

372

In Fig.7 the cross-correlation analysis between Δ GWL and average precipitation in the catchment is presented which suggests that the highest correlation happens at lag zero which indicates the time-lag between Δ GWL and precipitation is less than a month, meaning that precipitation needs less than a month to affect Δ GWL in the catchment. The short delay (lag-time) between precipitation and Δ GWL significantly depends on the catchment characteristics such as soil type, porosity, conductivity, land use, etc. and might be different for other locations, however it can provide straightforward, yet easy to implement information about the hydro(geo)logical system.



373

374

375

376

Fig.7 Cross-correlation between Δ GWL values and Precipitation (P) values showing time-lag between Δ GWL and precipitation is less than a month (the dashed lines show lag month during which the highest CCF value occurs between the two time-series)

377

5 Discussion

378

379

380

381

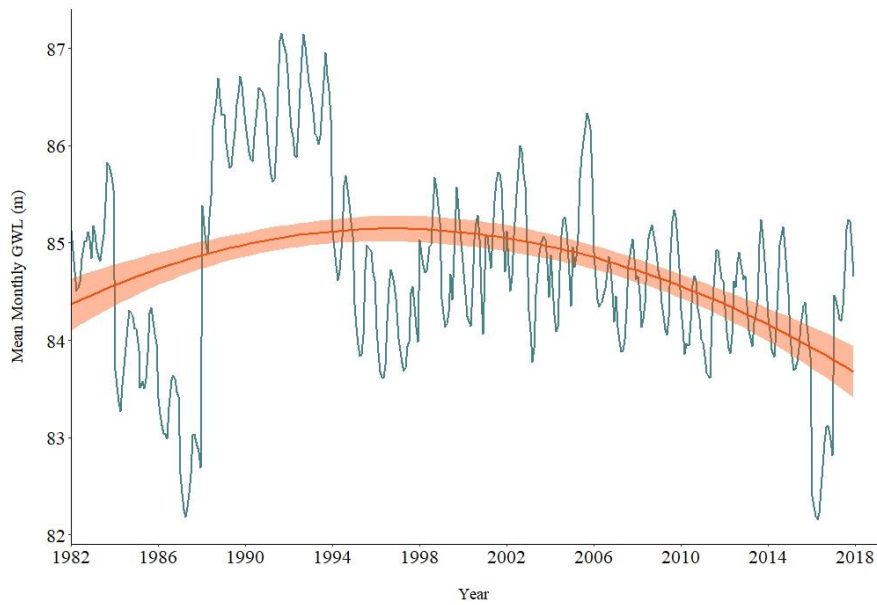
382

383

384

According to Figure 8 the mean monthly GWL has increased during 1988-1993 and decreased afterward (the trend line). The previous studies for the Harvey region reported decrease in GWL since 1980s (Ali et al., 2012; CSIRO, 2009; Kelsey et al., 2010) mainly due to extensive agricultural activities, urban development, and rainfall reduction. The current research confirmed these findings, showing that GWL in the catchment has decreased after a short period of increasing.

385



386

387

Fig.8 Mean Monthly trend of GWL during the study period

388

389

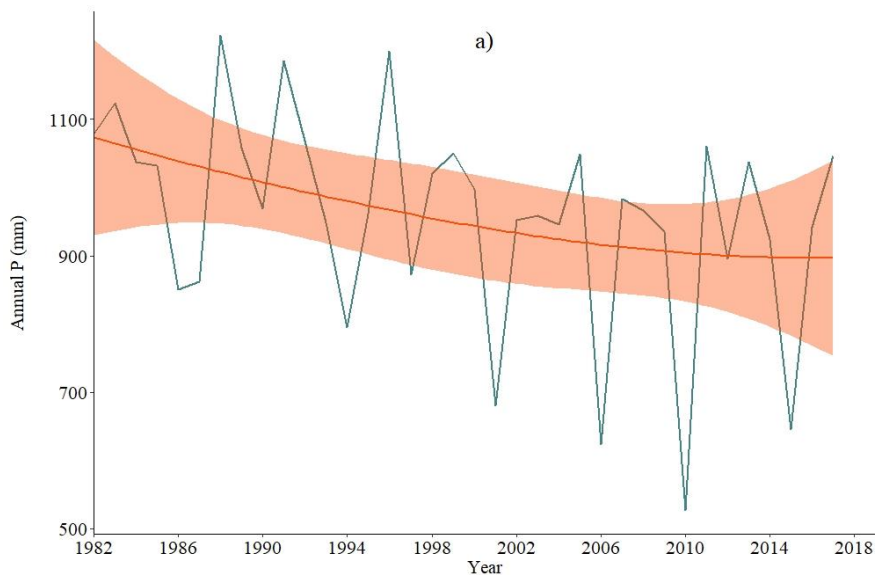
390

391

392

393

Figure 9 provides more detailed information. Although precipitation follows a decreasing trend (the red line), the annual precipitation during 1988 – 1993 is significantly above the average which coincides with those years in which GWL experienced a brief increase. The smooth bar around the trend lines for Figures 8 and 9 shows 95% level of confidence for the mean.



394

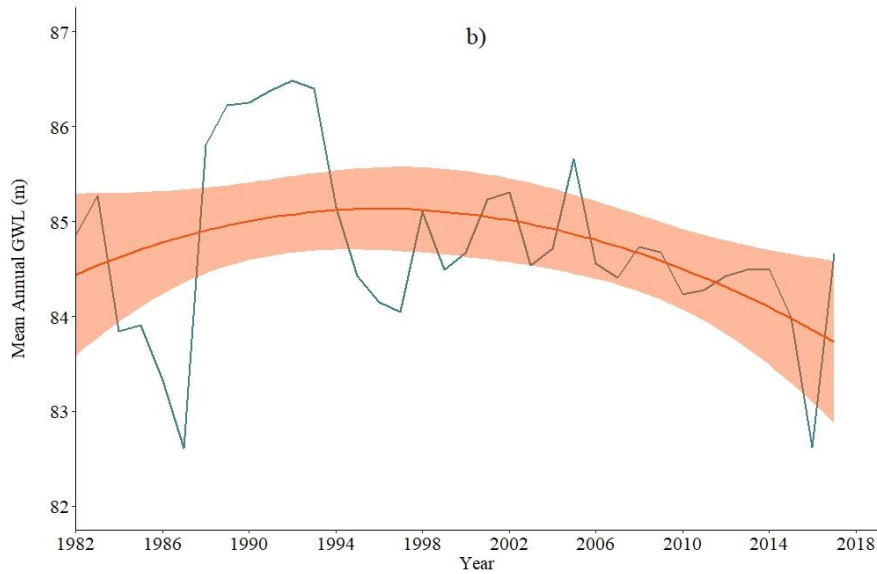


Fig.9 a) Annual Precipitation and b) Mean annual GWL trends during the study period

395
396

397 The Harvey Catchment, specifically in the coastal area, is reported to have a shallow
 398 water table. By deducting earth elevation from estimated GWL at each grid point, it was
 399 confirmed that the catchment is shallow, and water level almost stands within 10 meters below
 400 the earth surface. The deepest water table is located in the southeastern part of the catchment
 401 (Figure 4), where water level stands between 10 to 16 meters from the surface. Shallow
 402 catchments, especially in cases like Harvey, where the precipitation is highly seasonal, rejects
 403 recharging, after being full during winter time. Therefore the catchment is more vulnerable to
 404 water loss. On the other hand, rapid and extensive development in the study area causes higher
 405 rate of discharge than recharge, and hence results in more water loss. Decreasing water level
 406 increases the risk of ocean water intrusion, and deteriorates water quality (Ali et al., 2012).
 407 Because of the shallow groundwater, high permeability (i.e., high hydraulic gradient) and
 408 sandy soil of the catchment, a short time-lag between precipitation and Δ GWL was expected.
 409 The cross-correlation analysis showed the time-lag between the two time-series is less than a
 410 month. However, because of the chosen monthly time step in this study, it was not possible to
 411 detect the exact response time of Δ GWL time-series. In future studies, with a finer temporal
 412 grid (e.g., daily scale), it might be possible to track the possible weekly or daily time-lag.
 413 Although, due to the extensive computational process, probably, a shorter time period should
 414 be adopted.

415 The Rkriging method is a beneficial, yet, computationally extensive task. The model
 416 should perform the inversion covariance matrix, which makes the calculation process massive.
 417 Unlike spatial or temporal kriging, the method considers the time and space dependency of the

418 variables by building a correlation between the parameters so that even when some of the
419 spatial or/and temporal points are missing the uniform spatiotemporal estimation is carried on
420 (Varouchakis & Hristopulos, 2019).

421 The proposed method showed that GWL has decreased in the catchment, during the
422 study period. The estimated GWL provides valuable information about hydrogeological
423 condition of the catchment, and hence can be useful for predicting future change and
424 distinguishing potential environmental threats to the catchment (Ferdowsian & Pannell, 2009).
425 Furthermore, the GWL information is important to accurately quantify water extraction
426 capacity and amount of discharge and recharge to the groundwater system, which in return, is
427 essential for proposing sustainable water supply plan (John & John, 2019; Kotchoni et al.,
428 2019). Therefore, the outcome of this study is, also, useful for policymakers and water
429 resources manager in developing sustainable plans and sustainable groundwater management.
430 The present research is part of a more extensive study on the impact of climate change and
431 human activities on water resources. For the next phase of the study, outcome of the current
432 research will be applied to investigate water resources variations in the Harvey Catchment,
433 during 1982-2017. In the absence of hydrological modelling and complex dataset, this method
434 can provide valuable information. Moreover, the Rkriging method is a competent approach for
435 cases with sparse non-uniform data, in fields such as hydrology, pollution tracking or other
436 environmental studies.

437

438 **6 Conclusion**

439 As uniformly distributed groundwater data is not available, this study successfully
440 applies Rkriging method to investigate groundwater change in the Harvey Catchment, Western
441 Australia. The method displayed spatiotemporal interpolation between the non-uniform
442 observed groundwater data. To overcome the temporal and spatial gap in the data, a uniform
443 spatiotemporal grid was produced and accordingly monthly maps of the groundwater level for
444 the catchment were created. The proposed method confirmed the reported decreasing
445 groundwater level status in the catchment. In order to further investigate this reduction and its
446 correlation with temporal precipitation change, time-series analysis was performed. The results
447 showed there is a short time-lag between the precipitation and Δ GWL time-series (less than a
448 month), which is expected considering Harvey Catchment has relatively shallow groundwater
449 table. The proposed method can be used for other catchments where limited groundwater data

450 is available. It increases the spatiotemporal understanding of the studied parameters where
451 irregular temporal and spatial data is the only available information.

452

453 **Acknowledgment**

454 The hydrological data (including groundwater and precipitation) were acquired from
455 the website of Bureau of Meteorology (BOM) of Australia
456 (<http://www.bom.gov.au/waterdata/>). All the code writing and modeling was done in Rstudio
457 software, using the gstat, sp, spacetime and ggplot2 packages.

458 Comments and suggestions from the Editor and three anonymous reviewers are
459 gratefully acknowledged.

460

461 **Conflict of Interest Statement**

462 The authors declare no conflicts of interest.

463

464 **7 References**

465 Adigi, J. A. (2019). Spatio-temporal regression kriging for predicting rainfall from sparse
466 precipitation data in Ghana, University of Twente.

467 Al-Safi, H. I. J., Kazemi, H., & Sarukkalige, P. R. (2020). Comparative study of conceptual
468 versus distributed hydrologic modelling to evaluate the impact of climate change on
469 future runoff in unregulated catchments. *Journal of Water and Climate Change*, 11(2),
470 341-366.

471 Ali, R., McFarlane, D., Varma, S., Dawes, W., Emelyanova, I., Hodgson, G., & Charles, S.
472 (2012). Potential climate change impacts on groundwater resources of south-western
473 Australia. *Journal of Hydrology*, 475, 456-472.

474 Australian Bureau of Meteorology. Climate Data Online. Retrieved January 20, 2020, from
475 <http://www.bom.gov.au/climate/data/index.shtml>

476 Environmental Protection Authority (2008). Water Quality Improvement Plan for the Rivers
477 and Estuary of the Peel-Harvey System - Phosphorus Management, Environmental
478 Protection Authority, Perth, Western Australia.

479 Cai, Z., & Ofterdinger, U. (2016). Analysis of groundwater-level response to rainfall and
480 estimation of annual recharge in fractured hard rock aquifers, NW Ireland. *Journal of*
481 *Hydrology*, 535, 71-84.

482 CSIRO (2009) Groundwater yields in south-west Western Australia. A report to the Australian
483 Government from the CSIRO South-West Western Australia Sustainable Yields
484 Project. CSIRO Water for a Healthy Country Flagship, Australia.

- 485 CSIRO. (2009). Water yields and demands in south- west Western Australia. A report to the
 486 Australian Government from the CSIRO South- West Western Australia Sustainable
 487 Yields Project.
- 488 Dash, J., Sarangi, A., & Singh, D. (2010). Spatial variability of groundwater depth and quality
 489 parameters in the national capital territory of Delhi. *Environmental Management*, 45(3),
 490 640-650.
- 491 De Vries, J. J., & Simmers, I. (2002). Groundwater recharge: an overview of processes and
 492 challenges. *Hydrogeology Journal*, 10(1), 5-17.
- 493 Derakhshan, H., & Leuangthong, O. (2006). A Review of Separable Spatiotemporal Models of
 494 Regionalization.
- 495 Dimitrakopoulos, R., & Luo, X. (1994). Spatiotemporal modelling: covariances and ordinary
 496 kriging systems. In *Geostatistics for the next century* (pp. 88-93): Springer.
- 497 Duvert, C., Jourde, H., Raiber, M., & Cox, M. E. (2015). Correlation and spectral analyses to
 498 assess the response of a shallow aquifer to low and high frequency rainfall fluctuations.
 499 *Journal of Hydrology*, 527, 894-907.
- 500 Ferdowsian, R., & Pannell, D. (2009). Explaining long-term trends in groundwater
 501 hydrographs. Paper presented at the Proceedings of the 18th World IMACS/MODSIM
 502 Congress, Cairns, Australia.
- 503 Geniaux, G. (2017). Analyzing spatio-temporal data with R: everything you always wanted to
 504 know-but were afraid to ask. *Journal de la Société Française de Statistique*, 158(3), 124-
 505 158.
- 506 Goovaerts, P. (2000). Geostatistical approaches for incorporating elevation into the spatial
 507 interpolation of rainfall. *Journal of Hydrology*, 228(1-2), 113-129.
- 508 Graler, B., Pebesma, E., & Heuvelink, G. (2016). Spatio-temporal interpolation using gstat.
 509 *RFID Journal*, 8(1), 204-218.
- 510 Green, T. R., Taniguchi, M., Kooi, H., Gurdak, J. J., Allen, D. M., Hiscock, K. M., . . . Aureli,
 511 A. (2011). Beneath the surface of global change: Impacts of climate change on
 512 groundwater. *Journal of Hydrology*, 405(3-4), 532-560.
- 513 Guitton, A. (2004). Bound constrained optimization: Application to the dip estimation
 514 problem. Stanford Exploration Project. Retrieved from
 515 http://sepwww.stanford.edu/data/media/public/docs/sep117/antoine1/paper_html/node
 516 6.html
- 517 Guo, L., Lei, L., Zeng, Z.-C., Zou, P., Liu, D., & Zhang, B. (2014). Evaluation of spatio-
 518 temporal variogram models for mapping Xco 2 using satellite observations: A case
 519 study in China. *IEEE Journal of Selected Topics in Applied Earth Observations and*
 520 *Remote Sensing*, 8(1), 376-385.
- 521 Haylock, M., Hofstra, N., Klein Tank, A., Klok, E., Jones, P., & New, M. (2008). A European
 522 daily high- resolution gridded data set of surface temperature and precipitation for
 523 1950–2006. *Journal of Geophysical Research: Atmospheres*, 113(D20).
- 524 Hengl, T., Heuvelink, G. B., Tadić, M. P., & Pebesma, E. J. (2012). Spatio-temporal prediction
 525 of daily temperatures using time-series of MODIS LST images. *Theoretical and applied*
 526 *climatology*, 107(1), 265-277.
- 527 Hu, D., Shu, H., Hu, H., & Xu, J. (2017). Spatiotemporal regression Kriging to predict
 528 precipitation using time-series MODIS data. *Cluster Computing*, 20(1), 347-357.

- 529 John, R., & John, M. (2019). Adaptation of the visibility graph algorithm for detecting time lag
530 between rainfall and water level fluctuations in Lake Okeechobee. *Advances in Water*
531 *Resources*, 134, 103429.
- 532 Kazemi, H., Sarukkalige, R., & Badrzadeh, H. (2019). Evaluation of streamflow changes due
533 to climate variation and human activities using the Budyko approach. *Environmental*
534 *Earth Sciences*, 78(24), 713. doi:10.1007/s12665-019-8735-9
- 535 Kelsey, P., Hall, J., Kretschmer, P., Quinton, B., & Shakya, D. (2010). Hydrological and
536 nutrient modelling of the Peel-Harvey catchment. In: *Water Science Technical Series,*
537 *Report.*
- 538 Kim, J.-M., & Lee, J. (2017). Time series analysis for evaluating hydrological responses of
539 pore-water pressure to rainfall in a slope. *Hydrological Sciences Journal*, 62(9), 1412-
540 1421.
- 541 Kotchoni, D. V., Vouillamoz, J.-M., Lawson, F. M., Adjomayi, P., Boukari, M., & Taylor, R.
542 G. (2019). Relationships between rainfall and groundwater recharge in seasonally
543 humid Benin: a comparative analysis of long-term hydrographs in sedimentary and
544 crystalline aquifers. *Hydrogeology Journal*, 27(2), 447-457.
- 545 Larocque, M., Mangin, A., Razack, M., & Banton, O. (1998). Contribution of correlation and
546 spectral analyses to the regional study of a large karst aquifer (Charente, France).
547 *Journal of Hydrology*, 205(3-4), 217-231.
- 548 Learning, E. o. M. (2010). Leave-One-Out Cross-Validation. In C. Sammut & G. I. Webb
549 (Eds.), *Encyclopedia of Machine Learning* (pp. 600-601). Boston, MA: Springer US.
- 550 Lee, L., Lawrence, D., & Price, M. (2006). Analysis of water-level response to rainfall and
551 implications for recharge pathways in the Chalk aquifer, SE England. *Journal of*
552 *Hydrology*, 330(3-4), 604-620.
- 553 Lehmann, A., & Rode, M. (2001). Long-term behaviour and cross-correlation water quality
554 analysis of the river Elbe, Germany. *Water Research*, 35(9), 2153-2160.
- 555 Pebesma, E. J. (2004). Multivariable geostatistics in S: The gstat package. *Computers &*
556 *Geosciences*, 30(7), 683–691. <https://doi.org/10.1016/j.cageo.2004.03.012>
- 557 Rouhani, S., & Hall, T. J. (1989). Space-time kriging of groundwater data. In *Geostatistics* (pp.
558 639-650): Springer.
- 559 Ruibal-Conti, A. L. (2014). *Connecting Land to the Ocean: A Restrospective Analysis of*
560 *Nutrient Flux Pathways Within the Peel-Harvey Catchment-estuary System.* University
561 of Western Australia,
- 562 Ruybal, C. J., Hogue, T. S., & McCray, J. E. (2019). Evaluation of groundwater Levels in the
563 Arapahoe Aquifer using Spatiotemporal regression kriging. *Water Resources Research*,
564 55(4), 2820-2837.
- 565 Shi, L., Zhang, B., Wang, H.-x., Zhang, H.-j., Peng, Z.-h., & Li, J.-y. (2019). Investigation on
566 the causes of abnormal increase of water inflow in underground water-sealed storage
567 system. *Tunnelling and Underground Space Technology*, 87, 174-186.
- 568 Taylor, R. G., Scanlon, B., Döll, P., Rodell, M., Van Beek, R., Wada, Y., . . . Edmunds, M.
569 (2013). Ground water and climate change. *Nature Climate Change*, 3(4), 322-329.
- 570 Varouchakis, E. A., & Hristopulos, D. T. (2019). Comparison of spatiotemporal variogram
571 functions based on a sparse dataset of groundwater level variations. *Spatial Statistics*,
572 34, 100245.

- 573 Varouchakis, E., & Hristopulos, D. (2013). Comparison of stochastic and deterministic
574 methods for mapping groundwater level spatial variability in sparsely monitored basins.
575 *Environmental monitoring and assessment*, 185(1), 1-19.
- 576 Voss, S., Zimmermann, B., & Zimmermann, A. (2016). Detecting spatial structures in
577 throughfall data: The effect of extent, sample size, sampling design, and variogram
578 estimation method. *Journal of Hydrology*, 540, 527-537.
- 579 Yao, L., Huo, Z., Feng, S., Mao, X., Kang, S., Chen, J., . . . Steenhuis, T. S. (2014). Evaluation
580 of spatial interpolation methods for groundwater level in an arid inland oasis, northwest
581 China. *Environmental Earth Sciences*, 71(4), 1911-1924.

Conflict of Interest Statement

The authors declare no conflicts of interest.

The Authors certify that all authors have seen and approved the final version of the manuscript and warrant that the article is the authors' original work, hasn't received prior publication and isn't under consideration for publication elsewhere.